UNCLASSIFIED

AD 93852

Armed Services Technical Information Agenc

Reproduced by

DOCUMENT SERVICE CENTER

KNOTT BUILDING, DAYTON, 2, OHIO

This document is the property of the United States Government. It is furnished for the duration of the contract and shall be returned when no longer required, or upon recall by ASTIA to the following address: Armed Services Technical Information Agency, Document Service Center, Knott Building, Dayton 2, Ohio.

NOTICE: WHEN GOVERNMENT OR OTHER DRAWINGS, SPECIFICATIONS OR OTHER DATA ARE USED FOR ANY PURPOSE OTHER THAN IN CONNECTION WITH A DEFINITELY RELATEI GOVERNMENT PROCUREMENT OPERATION, THE U. S. GOVERNMENT THEREBY INCURS NO RESPONSIBILITY, NOR ANY OBLIGATION WHATSOEVER; AND THE FACT THAT THE GOVERNMENT MAY HAVE FORMULATED, FURNISHED, OR IN ANY WAY SUPPLIED THE SAID DRAWINGS, SPECIFICATIONS, OR OTHER DATA IS NOT TO BE REGARDED BY IMPLICATION OR OTHERWISE AS IN ANY MANNER LICENSING THE HOLDER OR ANY OTHER PERSON OR CORPORATION, OR CONVEYING ANY RIGHTS OR PERMISSION TO MANUFACTUR USE OR SELL ANY PATENTED INVENTION THAT MAY IN ANY WAY BE RELATED THERETO.

UNCLASSIFIED

AD No 23252
ASTIA FILE COPY

NEVIS - 24

NEVIS CYCLOTRON LABORATORIES

COLUMBIA UNIVERSITY
PHYSICS DEPARTMENT
Irvington-on-Hudson,
New York

FC

Joint ONR - AEC Program
Office of Naval Research Contract
Contract N6-ori-110 Task No. 1

R - 130
CU - 107
Nevis - 24

Nevis Cyclotron Laboratories
Columbia University
Physics Department
Irvington-on-Hudson,
New York

THE ELASTIC SCATTERING OF 78 MEV PIONS FROM COPPER

Ross E. Williams, Winslow F. Baker, and James Rainwater

CU-107-56-ONR-110-1-Physics

Submitted by Ross E. Williams
in partial fulfillment of the
requirements for the degree of
Doctor of Philosophy in the
Faculty of Pure Science,
Columbia University

March, 1956

Joint ONR-AEC Program
Office of Naval Research Contract
Contract N6-ori-110-Task No. 1

THE ELASTIC SCATTERING OF 77 MEV PIONS FROM COPPER* **

Ross E. Williams+, Winslow F. Baker, and James Rainwater

March, 1956

---

* This research is supported in part by the joint program of the Office of Naval Research and the Atomic Energy Commission.

** Submitted by Ross E. Williams in partial fulfillment of the requirements for the degree of Doctor of Philosophy in the Faculty of Pure Science, Columbia University.

+ Now at Paul Rosenberg Associates, Mount Vernon, New York

ABSTRACT

The angular distributions of 78 ± 5 Mev π^- and π^+ mesons scattered elastically from copper have been measured. The experimental results are compared with the distributions found from a range of exact optical model phase shift calculations using a complex attractive square well potential for $r < R_0$ (where $R_0 = 1.4A^{1/3} \times 10^{-13}$ cm) and the Coulomb potential for $r > R_0$. The effect of adding to the potential a term depending upon the gradient of the nuclear density, and thereby introducing a discontinuity in the matching of

logarithmic derivatives at $r = R_0$, is also explored. The optical model as well as several modified Born approximation calculations show reasonable agreement with the experimental curve in the forward direction and in the region of the first diffraction maximum. At backward angles the calculated curves show pronounced maxima and minima which do not appear experimentally, perhaps because incoherent transitions at these angles mask the true coherent distribution in the experimental measurement.

I. INTRODUCTION

The elastic[1] scattering of 78 ± 5 Mev π^- and π^+ by copper

---

[1] The sum of true elastic plus nearly elastic scattering is actually measured.

---

was measured to examine the pion angular distribution produced by a medium - heavy nucleus. This is one part of a program to explore variations in positive and negative pion differential cross sections over the range of available target nuclei. A recent measurement[2] of elastic pion scattering from lithium revealed a pronounced minimum and a strong backward rise

---

[2] R. E. Williams, J. Rainwater, A. Pevsner, Phys. Rev. 101, 412, (1956)

---

characteristic of the elementary pion-single nucleon angular distributions. For the (Z = 3) lithium nucleus an analysis was made in terms of a coherent addition of elementary scattering amplitudes using a modified impulse approximation analysis. An earlier experiment[3] had shown no pronounced

---

[3] A. Pevsner, J. Rainwater, R. E. Williams, and S. J. Lindenbaum, Phys. Rev. 100, 1419 (1955)

---

minimum and only a small backward rise for elastic pion

scattering from the somewhat heavier (Z = 13) aluminum nucleus. An optical model phase shift calculation using a complex square well potential showed strong maxima and minima for aluminum which did not appear in the experimental curves, but otherwise the general characteristics of the calculated curves at angles below that of the first diffraction minimum could be approximately matched to the experimental results. For the present experiment, copper (Z = 29) was chosen as a material of medium Z whose nuclear radius approximately equals the pion mean free path for absorption in nuclear matter. For the heavier copper nucleus the complex square well might be expected to better represent the overlapping fields of the individual nucleons, and the experiment was carried out with relatively high angular resolution and good statistical accuracy in an attempt to avoid masking whatever optical model diffraction effects might be present. The measured angular distribution shows some suggestion of a diffraction-like oscillation effect in the region of 40° to 80°. Optical model calculations have been made using a complex square well potential. The effect of including an added term which depends upon the gradient of the nuclear density[4] was also tested. When a square well potential is used the gradient term alters the boundary condition for matching inside and outside solutions at the nuclear surface.

[4] L. S. Kisslinger, Phys. Rev. 98, 761 (1955)

II. EXPERIMENTAL ARRANGEMENT

The scintillation counters and coincidence circuits used to measure pion angular distributions from the copper target are the same ones previously described for the pion experiments with lithium and aluminum targets. The arrangement of the scintillation counter telescopes and a description of the electronic circuitry have been given in earlier papers[2,3]. In brief summary, the telescopes are placed behind a focusing magnet in the 80 Mev pion exit channel of the 380 Mev Nevis synchrocyclotron, as shown in Figure 1. To measure angular distributions, counters 3 and 4 can be rotated vertically about the target position as a pivot point. Three fast (10^{-8} sec) coincidence circuits are used between various counter pair combinations in the two telescopes in such a manner as to reduce background due to random coincidences between counters to a low level; while a slower (10^{-7} sec) triple coincidence, operating on the output of the faster circuits, establishes the overall coincidence rate.

III. EXPERIMENTAL RESULTS

The measured angular distributions, together with the spreads in angular resolution, are shown for 78 Mev negative pions in Table I, and for 78 Mev positive pions in Table II. The $\pm$ quantities listed with the cross sections are the statistical standard deviations. The results are also shown in Figure 2. The many corrections to the raw counting data

required to arrive at the differential cross sections have been described in detail in the earlier papers[2,3]. These include adjustment for counting efficiency in the electronics, multiple Coulomb scattering in the target and copper absorber, incident beam width, finite counter size, π-μ decay after traversing the target, electron and μ meson contamination in the incident beam, stopping power of the target, nuclear absorption of full energy mesons in the target and copper absorber, low energy pions in the incident beam, etc. Plots of the values included in Tables I and II are shown in Figure 2. The π^- curve shows some evidence of a diffraction-like oscillation effect near the bottom of the initial decrease of $\frac{d\sigma}{d\Omega}$ in going from small to moderate angles. The points near 60^o appear as a relative bump on the curve that would be constructed by interpolating from the points on either side. This is the first evidence of such diffraction ''structure'' in the scattering of pions from complex nuclei, and provides an interesting feature for comparison with the results of optical model phase shift calculations.

IV. NUCLEAR MODELS

Watson[5] and Francis[6] have given general arguments for the validity of nuclear optical model potentials for pion scattering from nuclei. It is expected for light nuclei that the results

---

5 K. M. Watson, Phys. Rev. 89, 575 (1953)

6 N. C. Francis and K. M. Watson, Phys. Rev. 92, 291 (1953)

will be strongly influenced by characteristics of the elementary pion-nucleon amplitudes[4], whereas for heavier nuclei an optical model analysis using a complex interaction potential should become more valid. In a preceding paper[2] of this series a specific nuclear model was used with the impulse approximation to analyze the results of pion scattering from lithium in terms of the angularly dependent elementary pion-nucleon scattering amplitudes. To obtain definite individual particle nucleon wave functions, a simple harmonic nuclear well was assumed for the nucleons. The individual terms in the coherent addition of elementary scattering amplitudes from the various nucleons were weighted according to the ability of the struck nucleon to absorb the momentum recoil and remain in the same state in the simple harmonic nuclear well. Several obvious adjustments, such as relativistic solid angle and phase space corrections, were made. Corrections were also made at backward angles for the momentum distribution of the nucleons. By also taking into account the energy dependence of the elementary $f(\theta)$, fairly good agreement with the experimental angular distribution was obtained. The theoretical calculation was quite sensitive to the choice of such parameters as nuclear size and the approximations used in applying the correction factors. A best match with the experimental data corresponded to ''reasonable'' choices of these parameters.

Kisslinger has constructed nuclear scattering potentials directly from the elementary s and p wave amplitudes[4] and has

shown the importance of a surface term which arises from the p wave contribution to the elementary $f(\theta)$. The magnitude of the surface term depends upon $\nabla \rho$, where $\rho(r)$ is the nuclear density distribution. Variations in both range and shape of the nuclear density distribution about various favored distributions[7] have

[7] D. L. Hill and K. W. Ford, Phys. Rev. 94, 1617 (1954)

been made to fit both the experimental μ mesic x-ray data[8] and the

[8] V. Fitch and J. Rainwater, Phys. Rev. 92, 789 (1953)

electron scattering data.[9,10] Such studies have led to a favored

[9] Yennie, Ravenhall, and Wilson, Phys. Rev. 95, 500 (1954)

[10] R. Hofstadter, Proceedings of the Fifth Annual Rochester Conference on High-Energy Physics, Interscience Publishers, Inc., New York, 1955.

nuclear density distribution which is relatively uniform in the center region of the nucleus but tapers gradually to zero at the nuclear ''surface''. It should be noted, however, that the μ mesic x-ray and the electron scattering experiments give the charge distribution in the nucleus, whereas here we are interested in the average pion interaction as a function of r. This may be non-linear in nucleon density, may have a range extension, and may reflect differences in the neutron and proton distributions.

V. THEORY AND CALCULATIONS

We have performed phase shift optical model calculations using a constant complex square well potential within the nuclear radius ($r \leq R_0 = 1.4A^{1/3} \times 10^{-13}$ cm.), a Kisslinger type term at the surface, and a Coulomb potential beyond the nuclear radius. Exact solutions are obtained to the Klein Gordon equation in the form

$$\nabla^2\psi + \frac{(E - V)^2 - m^2c^4}{\hbar^2c^2}\psi = 0 \qquad (1)$$

Inside the nuclear surface $V = V_1 + iV_2$, at the surface $V_s\psi = -B\nabla\rho \cdot \nabla\psi$ where B is a negative constant, and beyond the surface $V = \frac{-Ze^2}{r}$. A range of inside potentials was chosen taking into account the increased Coulomb and nuclear contributions from the heavier copper nuclei compared with aluminum, for which the π^- potentials $V_1 = -30$ Mev and $V_2 = -10$ to -25 Mev seemed roughly appropriate.[3] The following sets of values were used:

(a) $V_1 = -25$ Mev, $V_2 = -20$ Mev
(b) $V_1 = -35$ Mev, $V_2 = -20$ Mev
(c) $V_1 = -45$ Mev, $V_2 = -20$ Mev
(d) $V_1 = -25$ Mev, $V_2 = -15$ Mev

Nuclear phase shifts were found in the conventional way by matching logarithmic derivatives of the regular and irregular Coulomb solutions (for $r > R_0$) to the spherical Bessel functions of complex argument inside the nucleus. The surface potential affected only the matching of logarithmic derivatives of the wave functions at the nuclear boundary. To be sure that

significant partial wave contributions were not neglected, ℓ values from 0 to 6 were included in the calculations. Actually contributions from partial waves with $\ell > 5$ should be small, and the results showed negligible contribution for $\ell > 6$.

For the radial part of the inside solution the complex propagation constant is given by

$$k_i^2 = \frac{(E - V_1 - iV_2)^2 - m^2c^4}{\hbar^2 c^2} \qquad (2)$$

where $V = V_1 + iV_2$ has been assumed somewhat arbitrarily to transform as the fourth component of a four vector, in analogy to the Coulomb potential for the outside solution. Wave functions for the inside Schrodinger equation are then the spherical Bessel functions

$$\psi_\ell = \frac{\chi_\ell}{r} = \sqrt{\frac{\pi}{2k_i r}} \; J_{\ell+\frac{1}{2}}(k_i r) \qquad (3)$$

from which, by the usual recurrence relations, the logarithmic derivatives at $r = R_0$ were found for ℓ values from 0 to 6.

If the small quadratic V term is neglected in (1), the outside Schrodinger equation reduces to the usual form

$$\nabla^2 \psi + \left(k_0^2 - \frac{2\alpha k_0}{r}\right) \psi = 0$$

where

$$k_0^2 = \frac{2m}{\hbar^2} E' \left(1 + \frac{E'}{2mc^2}\right)$$

and

$$E' = E - mc^2 = 78 \text{ Mev}$$

Choosing $R_0 = 1.414A^{1/3} \times 10^{-13}$cm., then $k_0R_0 = 4.8$ and

$$\alpha = \frac{mZe^2}{\hbar^2 k} \left(1 + \frac{E'}{mc^2}\right) = -.27487$$

for 78 Mev π^- mesons incident upon a copper nucleus. In order to represent an outgoing scattered wave superimposed upon an incident wave unmodified by the nuclear potential, the outside wave function must have the form

$$\mathscr{F}_\ell(\alpha, k_0R_0) = F_\ell(\alpha, k_0R_0) + [G_\ell(\alpha, k_0R_0) + iF_\ell(\alpha, k_0R_0)]\, e^{i\delta_\ell} \sin\delta_\ell \qquad (5)$$

where F_ℓ and G_ℓ are the regular and irregular hypergeometric wave functions. Values of F_ℓ were indirectly obtained from the NBS tables[11] which list $\Phi_\ell(\alpha, k_0R_0)$ and $C_0(\alpha)$, related to

---

[11] Tables of Coulomb Wave Functions, Volume I, National Bureau of Standards, Applied Mathematics Series 17, 1952.

F_ℓ by

$$F_\ell = C_\ell(\alpha)\, (k_0R_0)^{\ell+1}\, \Phi_\ell\, (\alpha, k_0R_0)$$

$$C_\ell(\alpha) = \frac{\sqrt{\ell^2 + \alpha^2}}{\ell(2\ell + 1)}\, C_{\ell-1}\, (\alpha)$$

and

$$C_\ell(-\alpha) = e^{\pi\alpha}\, C_\ell(\alpha)$$

Values of G_ℓ are not tabulated, except for positive values of α.[12]

---

[12] I. Bloch, M. M. Hull, Jr. A. A. Broyles, W. G. Bouricius, B. E. Freeman, and G. Breit, Rev. Mod. Phys. 23, 147 (1951)

Since our $\alpha = -.27487$, the existing tables could not be extrapolated from $\alpha = 0$ with sufficient accuracy. Therefore $G_1(\alpha, k_0R_0)$ was calculated from the very lengthy and slowly converging series expansions for G_ℓ. Other G_ℓ values were then found from

$$G_\ell = \frac{\ell(\ell^2 + \alpha^2)^{-\frac{1}{2}}}{F_{\ell-1}} + \frac{F_\ell G_{\ell-1}}{F_{\ell-1}}$$

F'_ℓ was calculated with the use of the recurrence relations

$$\ell F'_\ell = \sqrt{\ell^2+\alpha^2}\ F_{\ell-1} - (\frac{\ell^2}{k_0R_0} + \alpha)F_\ell \qquad \text{for } \ell \neq 0$$

$$(\ell+1)F'_\ell = [\frac{(\ell+1)^2}{k_0R_0} + \alpha]\ F_\ell - [(\ell+1)^2 + \alpha^2]^{\frac{1}{2}}\ F_{\ell+1} \quad \text{for } \ell = 0 .$$

G'_ℓ can then be found from the Wronskian equation

$$F'_\ell G_\ell - F_\ell G'_\ell = 1$$

The equation for the scattering amplitude[13] is

---

[13] L. I. Schiff, Quantum Mechanics, sec. 20, (McGraw Hill, New York, 1949)

$$f(\theta) = f_c(\theta) + \sum_{\ell=0}^{\infty} \frac{1}{k} (2\ell+1)\, e^{i(2\sigma_\ell+\delta_\ell)} \sin\delta_\ell\, P_\ell\, (\cos\theta) \quad (6)$$

where

$$f_c(\theta) = -\frac{\alpha}{2k\sin^2\frac{\theta}{2}}\, e^{-i\alpha \ln(\sin^2\frac{\theta}{2}) + 2i\sigma_0}$$

Values for σ_ℓ can be had from the tabulated[11] σ_0 values by means of the recurrence relation

$$\sigma_\ell = \sigma_{\ell-1} + \tan^{-1}\left(\frac{\alpha}{\ell}\right)$$

If the nucleon density is assumed constant within the nuclear radius (corresponding to a square well model) but drops to zero within a region $\gamma \to 0$ about the assumed radius, the matching condition at the boundary becomes[4]

$$\left[\frac{d\psi_\ell}{dr}\right]_+ = n \left[\frac{d\psi_\ell}{dr}\right]_- \quad (7)$$

where $n = 1 + \frac{2E}{\hbar^2 c^2} B\rho = 0.473$

E = meson total energy

ρ = nucleon density normalized so $\int \rho dV = 1$

$B = (2\pi)^3 At$

A = total number of nucleons

$t = \frac{-\hbar^2 c^2}{(2\pi)^2 E} \frac{3}{k^3} \eta_{++} \langle E_{3/2} \rangle \cdot \langle T_{3/2} \rangle = -.3611 \times 10^{-70}$ erg cm^5

$\eta_{++} = e^{i\delta_{++}} \sin\delta_{++}$ for both isotopic spin = 3/2 and j = 3/2 in pion-nucleon scattering

$E_{3/2}$ = spin projection operator for j = 3/2 in the pion-nucleon system

$T_{3/2}$ = isotopic spin projection operator for the T = 3/2 state of the pion-nucleon system.

Thus the new boundary matching condition, taking account of the logarithmic discontinuity, is

$$\frac{\mathscr{H}'_\ell}{\mathscr{H}_\ell} = \frac{(1-n)}{k_0 R_0} + n \frac{k_i}{k_0} \frac{\chi'_\ell}{\chi_\ell} \equiv h_\ell \qquad (8)$$

In our calculation we have used n = 0.5, 0.75, and 1.00 instead of the calculated 0.473 for the following reasons:

(a) Several choices of n values will better demonstrate the effect of the surface term.

(b) An exact choice for n is unnecessary, since (7) above has not been corrected for the difference in available phase space between pion-nucleon and pion-nucleus center of mass systems, or for the off-energy shell scattering which is actually taking place. Furthermore, the p state interaction between pion and nucleon gives rise to a mass like term and an ordinary potential term in the pion-nucleus Hamiltonian, in addition to the $\nabla\rho$ term. A consistent treatment would include expressions for these two additional terms; we have done so only through our phenomenological determination of the complex square well depths.

Nevertheless, a change in the angular distribution resulting from a change in n will at least be indicative of the effect of the surface potential contribution to the scattering.

The equation determining the nuclear phase shifts δ_ℓ from matching at the boundary is

$$e^{2i\delta_\ell} = \frac{(F'_\ell + iG'_\ell) - (F_\ell + iG_\ell)\, h_\ell}{-(F'_\ell - iG'_\ell) + (F_\ell - iG_\ell)\, h_\ell} \qquad (9)$$

From (9) δ_ℓ, and hence the partial wave coherent scattering amplitudes (6), can be found.

VI. RESULTS OF CALCULATIONS

The calculations, carried out on a desk calculator, are most easily studied by plotting $f(\theta)$ in the complex plane. Figures 3a and 3b show the complex $f(\theta)$ plots for $V_1 = -35$ Mev, $V_2 = -20$ Mev, and boundary matching factors n = 0.50, 0.75, and 1.00. The corresponding plot of the differential cross section is shown, along with the experimental curve, in Figure 4. Similar complex plots for $f(\theta)$ derived from $V_1 = -45$ Mev, $V_2 = -20$ Mev and the same range of n values are shown in Figures 5a and 5b. The corresponding angular distributions are shown in Figure 6. Figure 7 shows the calculated angular distributions for all four sets of complex potential wells previously mentioned, but for no discontinuity in logarithmic derivatives at the nuclear boundary (n=1).

It is obvious from Figure 7 that the calculated curves heavily overemphasize the diffraction maxima and minima in the angular distribution, relative to our experimental curve. However, it is difficult to say how strongly the experimental curve excludes such sharp prominences for strictly coherent scattering. In our experimental measurements, states of nuclear excitation $\lesssim$ 9 Mev can contribute to the measured cross section. Thus incoherent transitions such as spin flip and slightly inelastic scattering may be significant factors in the 10 mb. differential cross sections observed at backward angles. Furthermore, our angular resolution of $\pm$ 3.9° to 6.4° would tend to smooth out any sharp maxima and minima which might exist in the purely coherent angular distribution. Finally, a considerable damping of the calculated diffraction maxima and minima can probably be expected from a more reasonable nuclear model which abandons the sharp edged square well for a nuclear density distribution tapered toward the edge. Calculations with such a model require the use of electronic computers and were not attempted here.

The theoretical and experimental curves are best compared on the basis of the diffraction-like oscillation in the region from 40° to 80° and the height and slope of the curves at angles smaller than 40°. From Figure 7 it would seem that best agreement with the angular location of the first ''hump'' in the experimental curve might be obtained with the complex potential $V = (-45 - i\ 20)$ Mev, although the first maximum in the $V = (-35 - i\ 20)$ Mev calculated curve is only slightly

displaced toward larger angles relative to the experimental curve. (If a smaller nuclear radius or values of n less than unity are assumed, the location of the calculated first diffraction maximum will be shifted toward still larger angles.) The maximum in the calculated curves at 55° to 60° is not simply the result of interference between the Coulomb scattering amplitude and a monotonically decreasing nuclear scattering amplitude. The maximum would still be present as part of the diffraction pattern produced by the complex square well if the Coulomb potential were absent, although it would then be somewhat modified in amplitude and shifted in angular location.

At angles smaller than 40°, both the V = (-45 - i 20) Mev and V = (-35 - i 20) Mev calculated curves agree fairly well with the experimental values. In this region the partial wave scattering amplitudes are adding roughly in phase and interference effects between the various partial wave contributions, which may be sensitive to the assumed nuclear shape, are less important. Taking into account the slight lowering of $\frac{d\sigma}{d\Omega}$ brought about by adding a surface term to the potential (decreasing n from unity), slightly better agreement for a range of n values at forward angles is had with the potential V = (-45 - i 20) Mev than with V = (-35 - i 20) Mev. In the backward direction the curve for V = (-45 - i 20) Mev also stands higher and closer to the experimental curve, but it is in this region that incoherent scattering may be dominant and comparisons therefore less valid.

In comparing the calculated and experimental angular distributions it is difficult to assign a particular choice to n, which determines the discontinuity in logarithmic derivatives at the nuclear boundary. The choice of n is sensitive to the locations of maxima and minima in the backward direction, but since these are not clearly apparent in the experimental curve they are not useful criteria. As n is decreased from unity the first minimum and subsequent maximum in the calculated curves are damped and displaced slightly toward larger angles. The plots of $f(\theta)$ in the complex $(q + ip)$ plane in Figures 3 and 5 show how this is brought about. The complex $f(\theta)$ plots also show that changes in location and magnitude of maxima and minima at larger angles are not easily predicted as n varies. The locations and depths of the minima are determined by where and how close the $f(\theta)$ plots swing toward the origin as n is varied, and from Figures 3 and 5 it is seen that these features vary in a complex manner. In Figures 4 and 6 a higher backward cross section is obtained for the smallest n ($n = 0.5$), but this value of n does not allow a good match with the experimental curve in the region of the first diffraction maximum. Values of n from 0.75 to 1.00 appear to be favored when matching at the first diffraction maximum.

Optical model calculations were not made to fit the π^+ experimental distribution. However, the statistically weak experimental points at 50^o and 60^o suggest that a maximum may not be present in the π^+ curve in this region.

The total reaction cross section has also been calculated from the partial wave nuclear phase shifts for each of the real and imaginary square well potentials and boundary matching factors already discussed. Results are shown in Table III. For most values of the potentials, σ_r is slightly larger than the copper geometric cross section of 1006 mb (assuming $R_0 = 1.414\ A^{1/3} \times 10^{-13}$ cm). A similar result was found in the optical model study of pion scattering from aluminum[3]. Although the geometric cross section is the limit for absorption in the simple Fernbach, Serber, Taylor treatment,[14]

---

[14] Fernbach, Serber, and Taylor, Phys. Rev. 75, 1352 (1949)

---

much larger than geometric cross sections become possible with a partial wave analysis. The corresponding mean free paths for absorption, $\lambda_a = \frac{1}{2k_2}$, are all in the neighborhood of 4×10^{-13} cm.

We have also made two modified Born approximation calculations for scattering from a copper target (linear superposition of scattering amplitude contributions from the different nucleons) in order to compare with the results of the exact phase shifts of the optical model as well as to aid in the choice of well depths for the lengthier optical model calculations. Although the normal first Born approximation does not take into account attenuation effects or the difference in propagation constants inside and outside the nucleus, it

does make allowance for non-isotropic scattering from each element of nuclear matter, and coherently combines the scattering contributions from all parts of the nucleus according to a weighting function $f_b(\theta)$ which is found from the nuclear density distribution. Thus the total scattering amplitude $f(\theta)$ can be written as $f_a(\theta)\ f_b(\theta)$, where $f_a(\theta)$ is the nuclear volume times the Born contribution to the scattering amplitude per unit volume of nuclear matter, and $f_b(\theta)$, the nuclear density weighting function, gives the effect of the finite nuclear size. It is given[3] by

$$f_b(\theta) = \int_0^\infty r^2\, \rho(r)\, \frac{\sin qr}{qr}\, dr$$

Our modifications to this usual Born approximation have already been described,[15] and are briefly noted below.

---

[15] A. Pevsner and J. Rainwater, Phys. Rev. 100, 1431 (1955)

Modified Born Approximation A

$f_b(\theta)$ is modified to the extent of using $q_1 = 2k_1 \sin\frac{\theta}{2}$ instead of $q_0 = 2k_0 \sin\frac{\theta}{2}$, where k_0 and $k_i = k_1 + i\,k_2$ are the values of k at $r = \infty$ and $r < R_0$ respectively. This change brings the calculated diffraction minima to about the same angular positions as in the exact phase shift calculations. Also the interior parts of the nucleus are weighted less heavily by using an attenuation factor $e^{-k_2(R_0-r)}$. Thus

$$f_b(\theta) = \frac{3}{R_0^3} \int_0^{R_0} r^2 \frac{\sin q_1 r}{q_1 r} e^{-k_2(R_0-r)} dr$$

while

$$f_a(\theta) = \frac{2m}{\hbar^2} \left[\frac{Ze^2}{q_0^2} + \frac{1}{3} R_0^3 (V_1 + iV_2) \right]$$

Plots for the modified Born approximation A are shown in Figure 8 for three of the four sets of potentials for which the exact phase shift calculations were performed. Comparison with Figure 7 shows that the phase shift and modified Born approximation results are very similar. The minima are more pronounced and the entire curve somewhat lower in the Born case. Angles for the minima are nearly the same, but slightly smaller in the Born approximation.

Modified Born Approximation B

This is nearly the same as Born approximation 4 of Ref. 15. We no longer separate $f(\theta)$ into $f_a(\theta)$ and $f_b(\theta)$ factors, but instead calculate one scattering amplitude f_i for $r < R_0$ and another f_0 for $r > R_0$, and then combine the two coherently: $f = f_i + f_0$. In f_i, q_i again replaces q_0 (as opposed to the procedure of Ref. 15) and the nuclear attenuation factor also appears. Thus

$$f_i = -\frac{2m}{\hbar^2} \int_0^{R_0} r^2 \frac{\sin q_1 r}{q_1 r} (V_1 + i V_2) e^{-k_2(R_0-r)} dr$$

However in f_0, in which only the Coulomb potential appears, the nuclear attenuation factor is dropped and the outside $q = q_0$ is used.

$$f_0 = \frac{2m}{\hbar^2} \int_{R_0}^{\infty} \frac{\sin q_0 r}{q_0 r} \frac{Ze^2}{r} \, dr$$

Choosing a nuclear potential V =(-30 - i 20)Mev leads to the dotted curve in Figure 8. By interpolating between the curves of Figure 8, it is easily seen that the two modified Born approximations agree fairly well, and, with regard to angular locations of maxima and minima, both are fairly good approximations to the exact phase shift results.

VII. CONCLUSIONS

Taking into account the limited experimental angular and energy resolution, reasonably good agreement is obtained for angles up to 80° between the experimental distribution and calculated curves for V = (-45 - i20) Mev and V = (-35 - i20) Mev. The calculated curves for V = (-45 - i20) Mev give slightly better agreement with the magnitude of $\frac{d\sigma}{d\Omega}$ in the forward direction and the angular location of the first diffraction maximum. However, the calculated results are expected to be sensitive to the choice of nuclear radius, chosen here as $R_0 = 1.414 \, A^{1/3} \times 10^{-13}$cm, and the shape of the nuclear density distribution. Introducing a discontinuity in the logarithmic derivative matching at the nuclear surface has a pronounced effect upon the shape of the calculated curves, but n values less than about 0.75 do not

appear to improve the agreement with the experimental distribution, at least when applied to the square well model. At backward angles where incoherent transitions may mask the elastic scattering, the predicted maxima and minima do not appear experimentally. It is expected that a more reasonable nuclear model with a tapered edge, and an improvement in the experimental angle and energy resolution, may account for a large part of the discrepancy that still exists.

The authors wish to thank Miss Hilda Oberthal and Dr. Manfred Kochen for their aid in carrying out parts of the optical model phase shift calculation, and Mr. Ronald Rockmore for discussions concerning the gradient term in the potential. We are also indebted to the members of the Nevis Cyclotron operating and maintenance staffs for their continuous assistance during the experimental measurements.

FIGURE CAPTIONS

1. Experimental arrangement.

2. Experimental angular distribution for 78 Mev π^- and π^+ scattering from copper.

3a. Plot of $2k_0 f = q + ip$ for optical model phase shift analysis of π^- scattering from $\theta = 20^\circ$ to 80°, where $|f|^2 = \frac{d\sigma}{d\Omega}$. Curves are for $V_1 = -35$ Mev, $V_2 = -20$ Mev, and for wave function logarithmic derivative matching factors of n = 0.5, 0.75, and 1.00.

3b. Plot of $2k_0 f = q + ip$ for $\theta = 40^\circ$ to 160°, $V_1 = -35$ Mev, $V_2 = -20$ Mev, and n = 0.50, 0.75, 1.00.

4. Optical model solutions: angular distribution for 77 Mev π^- mesons scattered by copper for $V_1 = -35$ Mev, $V_2 = -20$ Mev. a) n = 1.00; b) n = 0.75; c) n = 0.50.

5a. Plot of $2k_0 f = q + ip$ for $\theta = 20^\circ$ to 80°, $V_1 = -45$ Mev, $V_2 = -20$ Mev, and n = 0.50, 0.75, 1.00.

5b. Plot of $2k_0 f = q + ip$ for $\theta = 40^\circ$ to 160°, $V_1 = -45$ Mev, $V_2 = -20$ Mev, and n = 0.50, 0.75, 1.00.

6. Optical Model solutions: angular distribution for 77 Mev π^- mesons scattered by copper for $V_1 = -45$ Mev, $V_2 = -20$ Mev. a) n = 1.00; b) n = 0.75; c) n = 0.50.

FIGURE CAPTIONS - continued

7. Optical model solutions: angular distribution for 78 Mev π^- mesons scattered from copper, for:

   a) $V_1 = -45$ Mev, $V_2 = -20$ Mev, $n = 1$

   b) $V_1 = -35$ Mev, $V_2 = -20$ Mev, $n = 1$

   c) $V_1 = -25$ Mev, $V_2 = -20$ Mev, $n = 1$

   d) $V_1 = -25$ Mev, $V_2 = -15$ Mev, $n = 1$

8. Modified Born approximation results: angular distribution of 78 Mev π^- mesons scattered by copper, for:

   a) $V_1 = -45$ Mev, $V_2 = -20$ Mev, Modified Born approximation A

   b) $V_1 = -35$ Mev, $V_2 = -20$ Mev, Modified Born approximation A

   c) $V_1 = -25$ Mev, $V_2 = -20$ Mev, Modified Born approximation A

   d) $V_1 = -30$ Mev, $V_2 = -20$ Mev, Modified Born approximation B

TABLE CAPTIONS

I. Experimental angular distribution of 78 Mev π^- mesons scattered from copper.

II. Experimental angular distribution of 78 Mev π^+ scattered mesons from copper.

III. Calculated optical model reaction (total minus coherent) cross sections for 78 Mev:

$$k_i = k_1 + ik_2 \ , \quad V = V_1 + iV_2$$

$$R_0 = 5.658 \times 10^{-13} \text{ cm}$$

$$k_0 R_0 = 4.80$$

$$\pi R_0^2 = 1006 \text{ mb.}$$

TABLE I

θ_{lab}	$\frac{d\sigma}{d\Omega}$ (mb)
20 ± 4.8^{o}	1459 ± 89
25.25 ± 4.9^{o}	747 ± 78
30 ± 4.6^{o}	385 ± 31
34.5 ± 3.9^{o}	177 ± 27
40 ± 3.9^{o}	59.4 ± 5.5
44.5 ± 4.2^{o}	57.5 ± 13.2
47 ± 4.2^{o}	41.4 ± 5.0
50 ± 4.3^{o}	36.1 ± 3.6
55 ± 4.3^{o}	33.1 ± 3.7
57.5 ± 5.8^{o}	31.3 ± 4.5
60 ± 4.4^{o}	27.7 ± 1.6
70 ± 5.8^{o}	12.12 ± 0.89
75 ± 5.4^{o}	11.52 ± 1.18
77 ± 6.5^{o}	11.74 ± 2.37
80 ± 5.1^{o}	12.01 ± 0.81
89 ± 5.3^{o}	11.58 ± 0.84
100 ± 5.7^{o}	10.39 ± 0.84
110 ± 6.0^{o}	9.13 ± 0.74
120 ± 5.9^{o}	10.19 ± 1.46
130 ± 6.4^{o}	9.95 ± 1.14
145 ± 4.4^{o}	11.04 ± 1.41

TABLE II

θ_{lab}	$\frac{d\sigma}{d\Omega}$ (mb)
15 ± 2.9^{o}	1882 ± 342
20 ± 5.0^{o}	748 ± 96
30 ± 4.2^{o}	267 ± 44
40 ± 4.2^{o}	63.3 ± 13.4
50 ± 4.3^{o}	30.2 ± 8.6
60 ± 5.9^{o}	16.2 ± 6.1
110 ± 6.5^{o}	8.29 ± 0.84

TABLE III

Case		n = 1				n = .75		n = .50	
V_1 (Mev)		-25	-25	-35	-45	-35	-45	-35	-45
V_2 (Mev)		-15	-20	-20	-20	-20	-20	-20	-20
k_1R_0		5.705	5.711	6.056	6.396	6.056	6.396	6.056	6.396
k_2R_0		.5257	.7001	.6874	.6766	.6874	.6766	.6874	.6766
$\lambda\!\!\!^{-}_a$ (10^{-13}cm)		5.38	4.04	4.12	4.21	4.12	4.21	4.12	4.21
$(2\ell+1)\pi\lambda\!\!\!^{-2}$	$\sigma_{r\ell}$								
(43.6)	σ_{r0}(mb)	39	41	39	38	42	41	44	43
(131)	σ_{r1}	113	121	126	129	117	123	99	107
(218)	σ_{r2}	175	191	182	181	195	188	201	184
(306)	σ_{r3}	274	294	285	252	295	288	282	301
(393)	σ_{r4}	266	297	350	384	311	357	248	297
(480)	σ_{r5}	98	122	158	208	145	187	121	151
(567)	σ_{r6}	17	23	27	34	26	32	23	27
$\sum_{\ell=0}^{6} \sigma_{r\ell} = \sigma_r$		982	1089	1167	1226	1131	1216	1018	1110

$\pi R_0^2 = 1006$

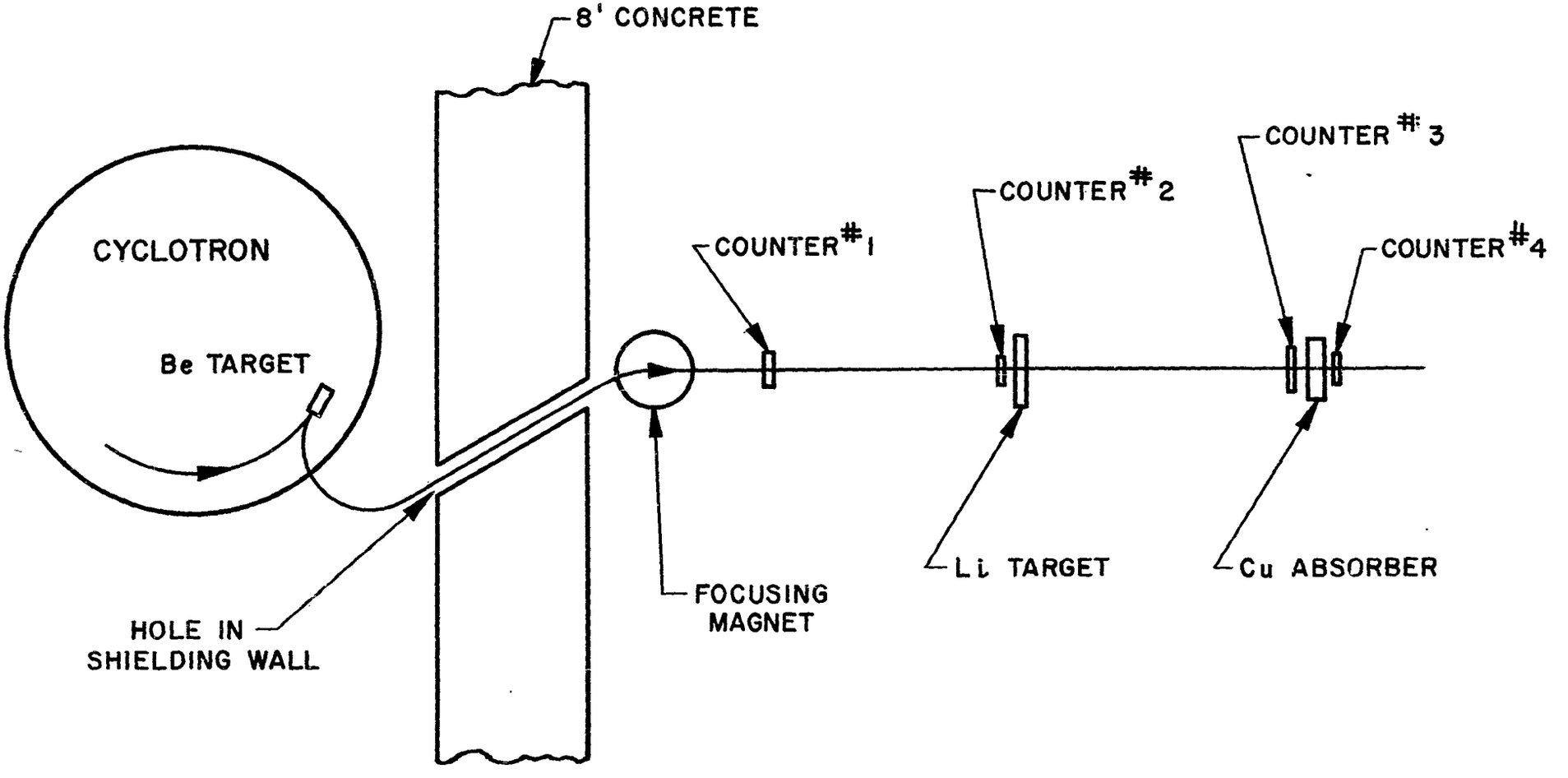

Fig. 1. Experimental Arrangement

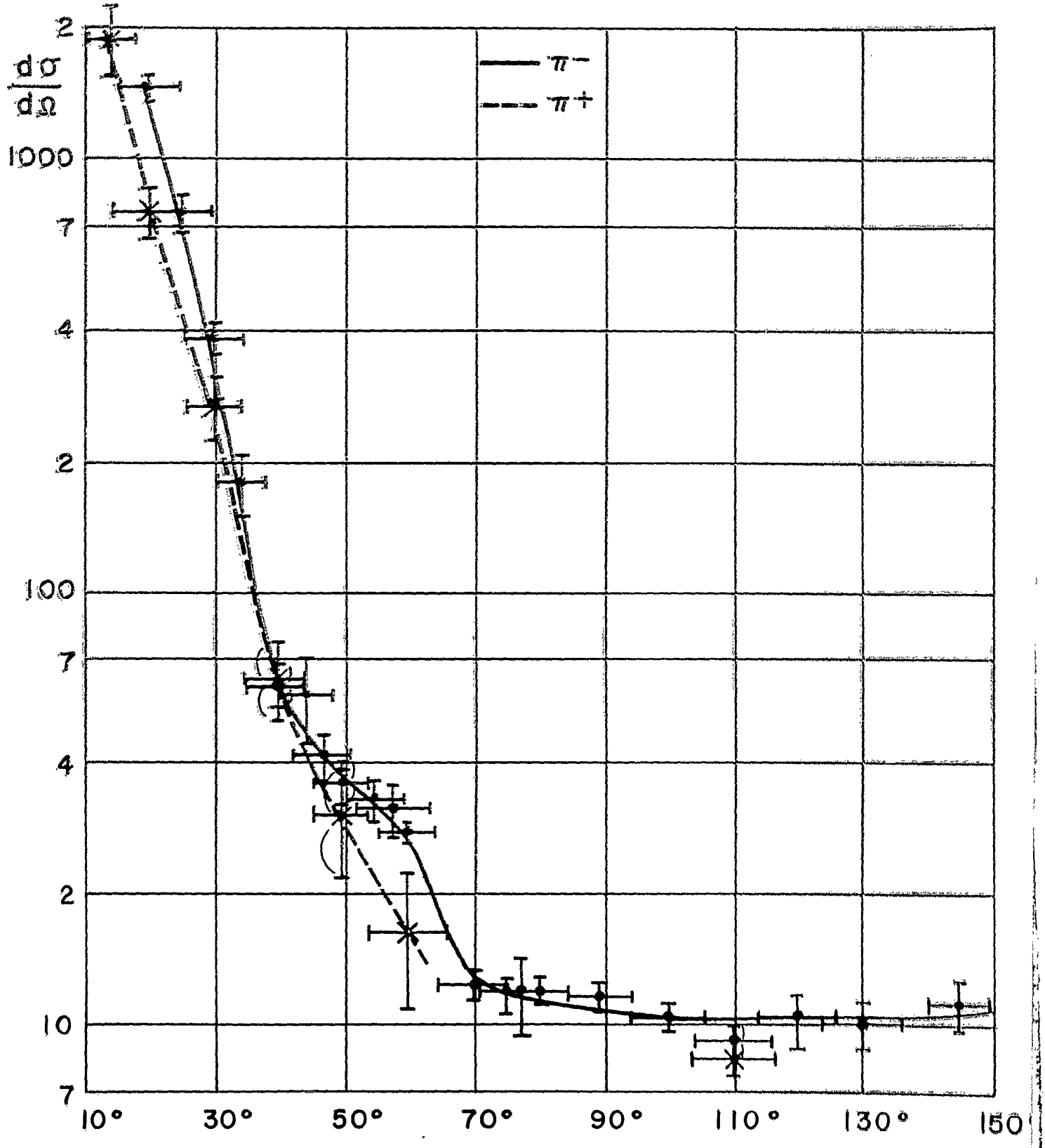
dσ/dΩ
2
1000
7
4
2
100
7
4
2
10
7
π−
π+
10°
30°
50°
70°
90°
110°
130°
150

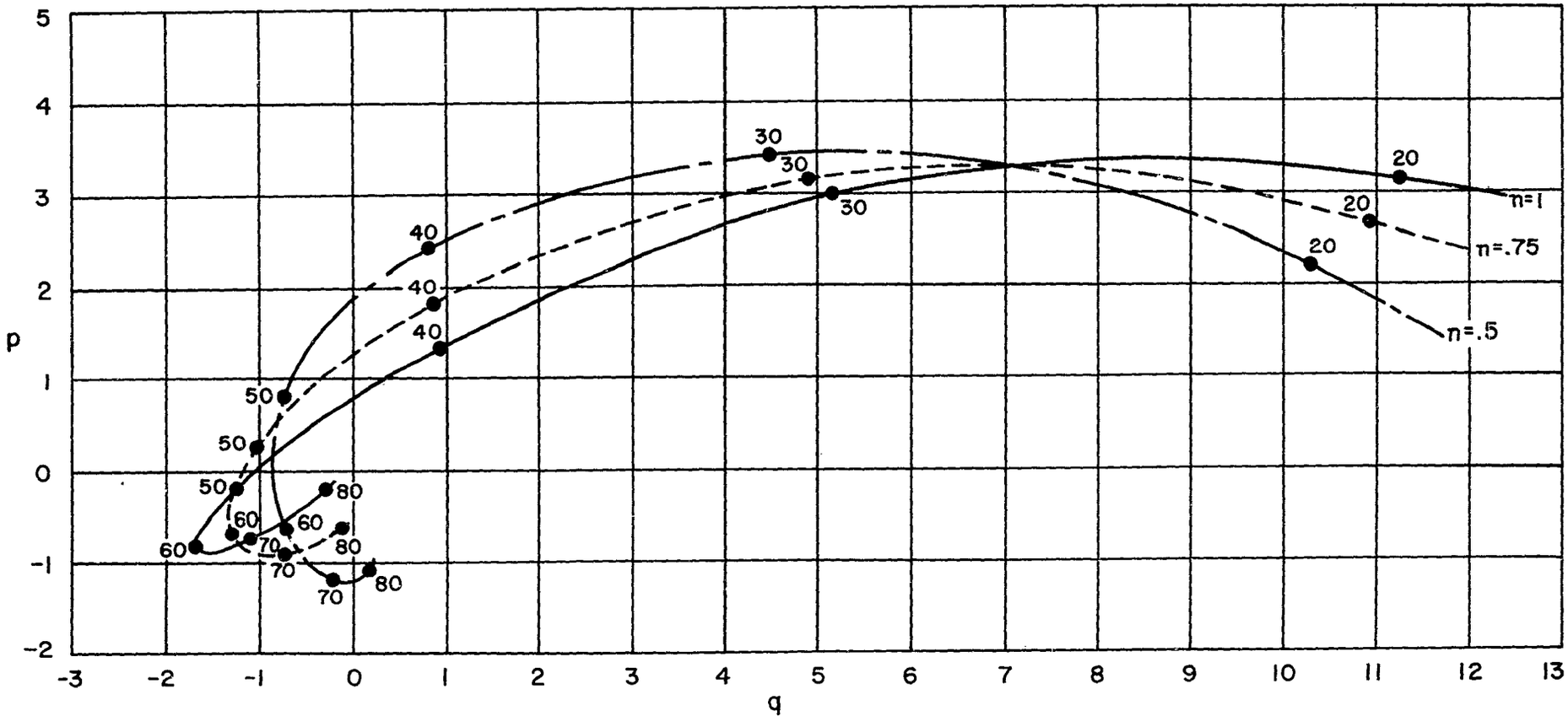
p
q
n=1
n=.75
n=.5
30
30
30
20
20
20
40
40
40
50
50
50
60
60
60
70
70
70
80
80
80

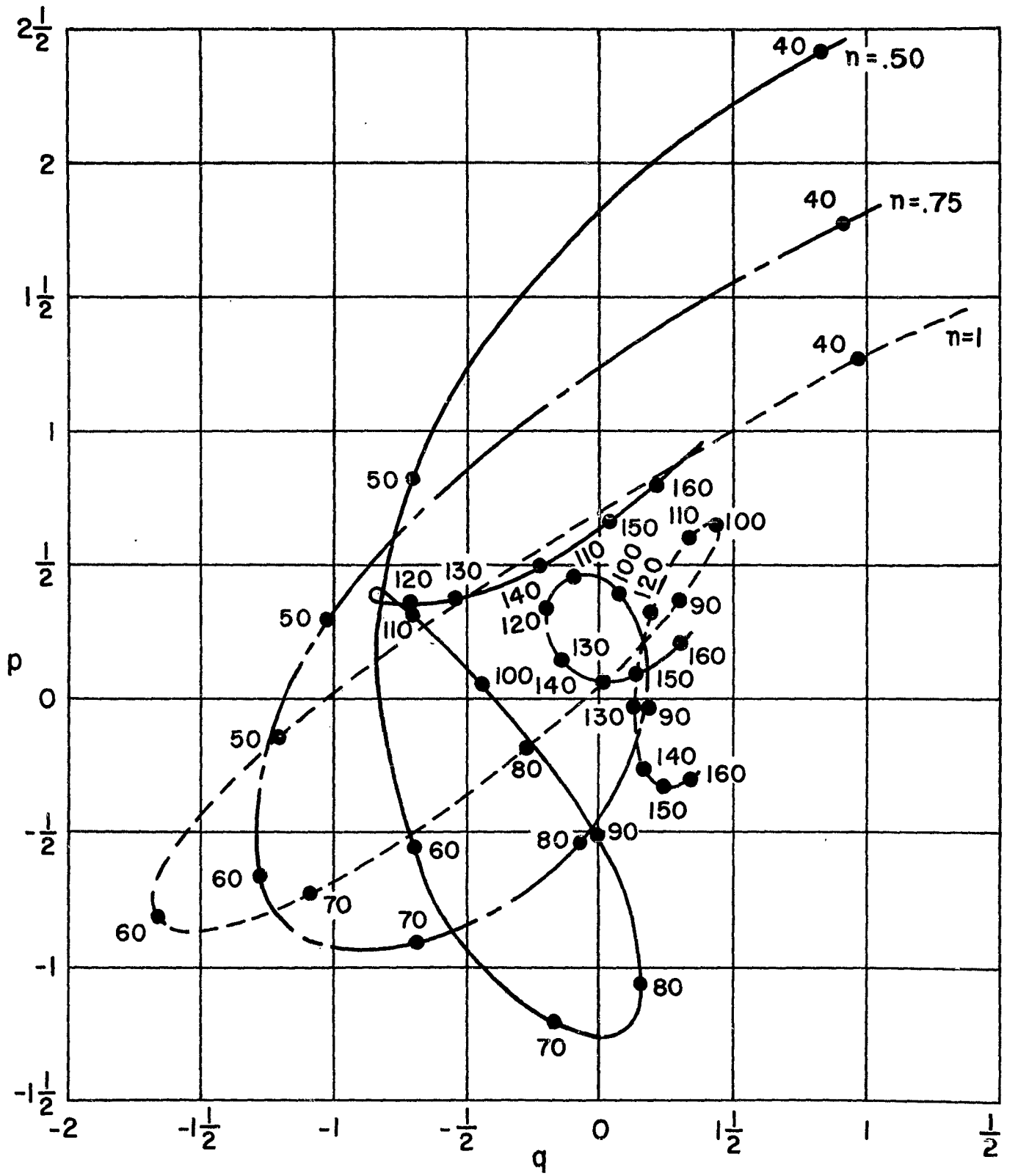
n=.50
n=.75
n=1
p
q
2½
2
1½
1
½
0
-½
-1
-1½
-2
-1½
-1
-½
0
1½
1
½
40
50
60
70
80
90
100
110
120
130
140
150
160

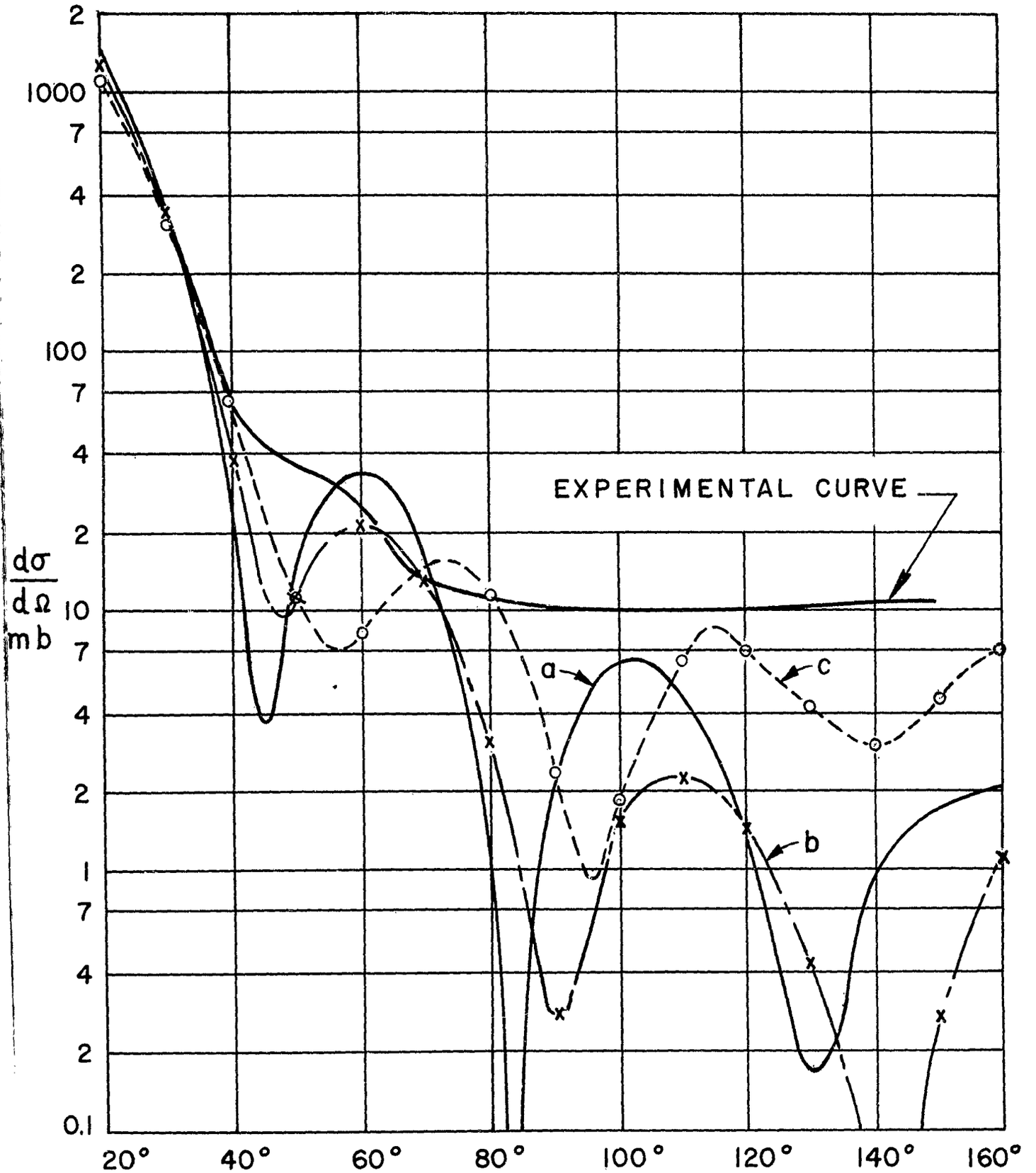
2
1000
7
4
2
100
7
4
2
10
7
4
2
1
7
4
2
0.1
dσ/dΩ mb
EXPERIMENTAL CURVE
a
b
c
20°
40°
60°
80°
100°
120°
140°
160°

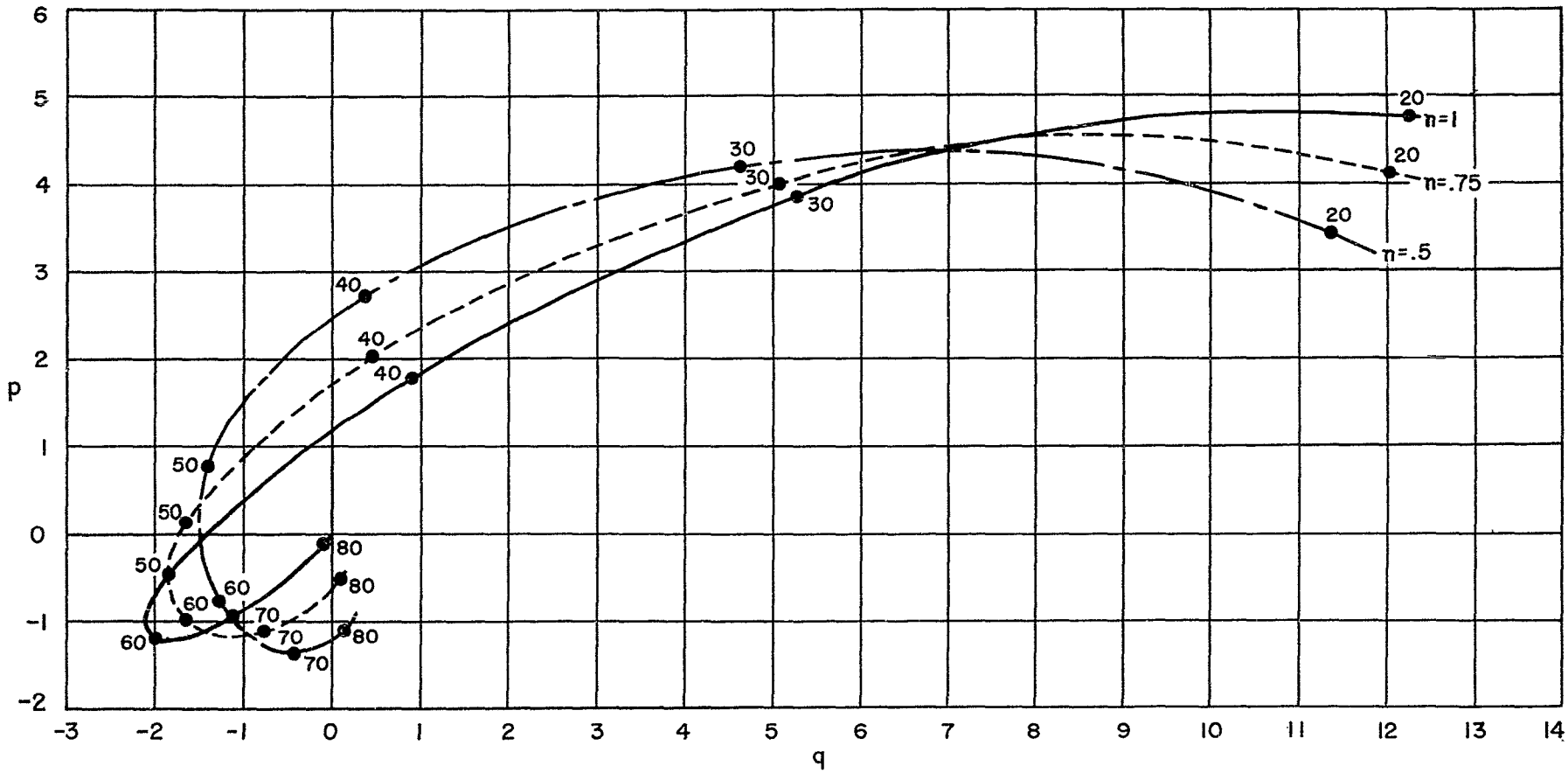
p
q
n=1
n=.75
n=.5
20
30
40
50
60
70
80

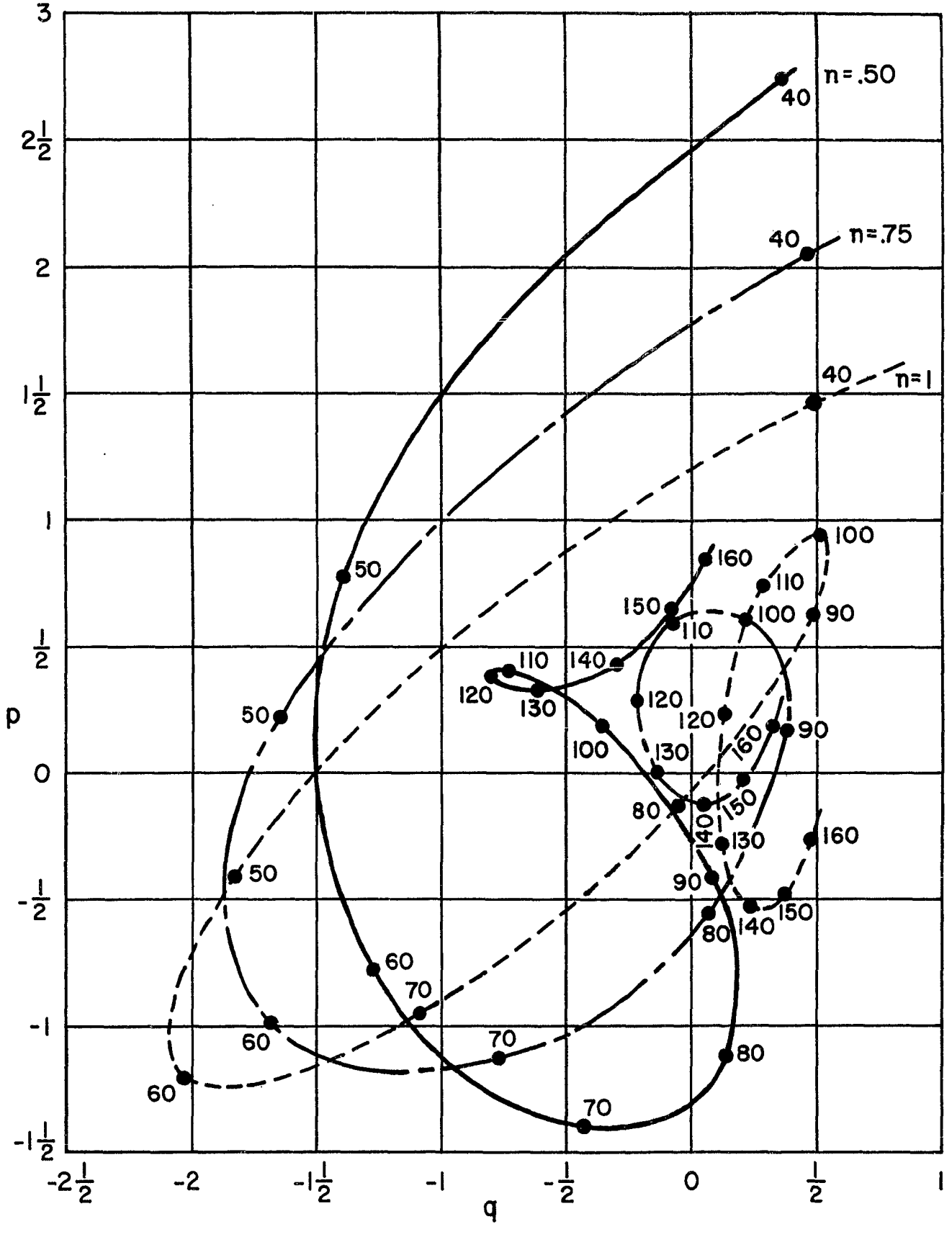
n=.50
n=.75
n=1
p
q
3
2½
2
1½
1
½
0
-½
-1
-1½
-2½
-2
-1½
-1
-½
0
½
1
40
50
60
70
80
90
100
110
120
130
140
150
160

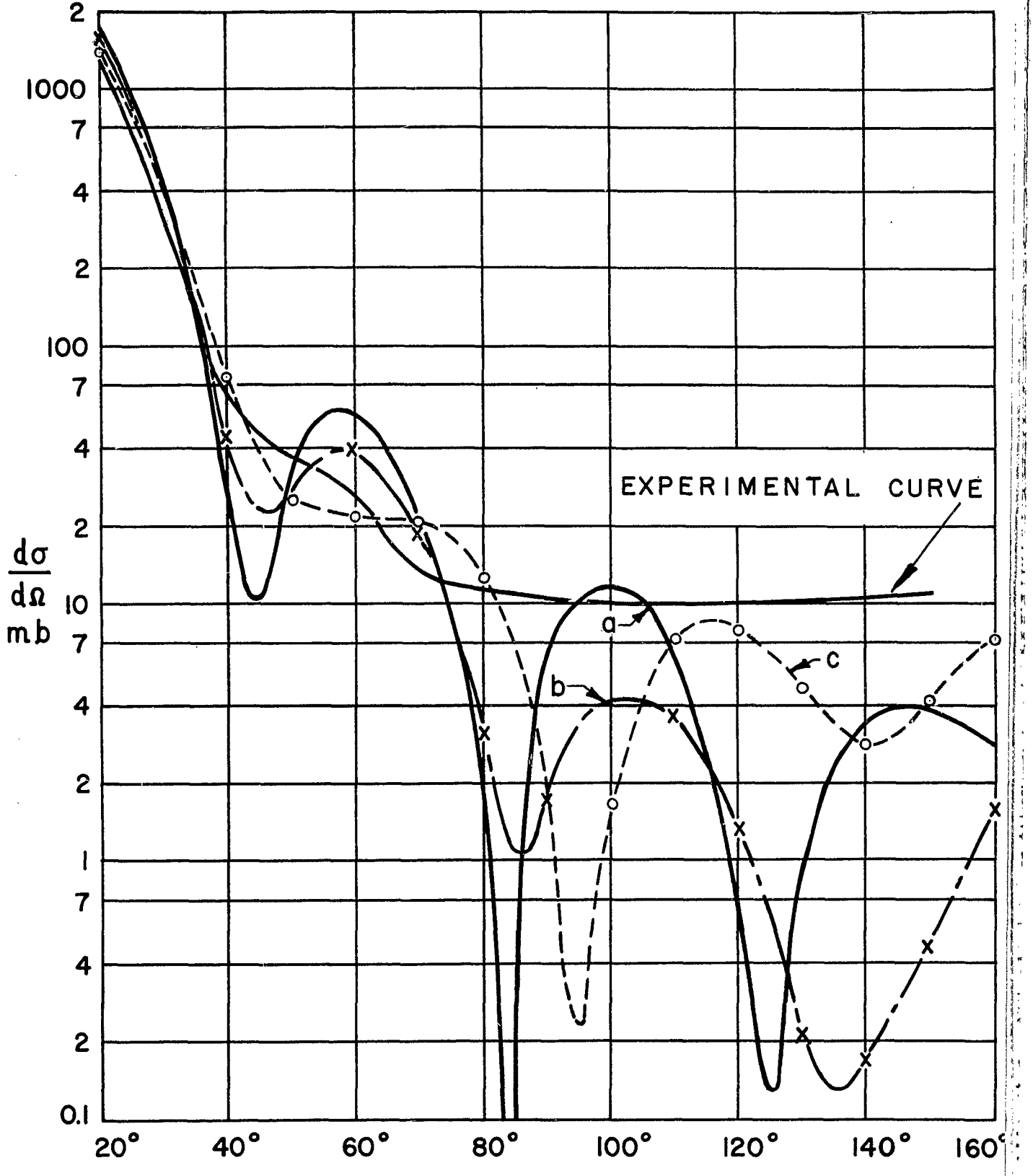
2
1000
7
4
2
100
7
4
2
10
7
4
2
1
7
4
2
0.1
dσ/dΩ mb
EXPERIMENTAL CURVE
a
b
c
20°
40°
60°
80°
100°
120°
140°
160°

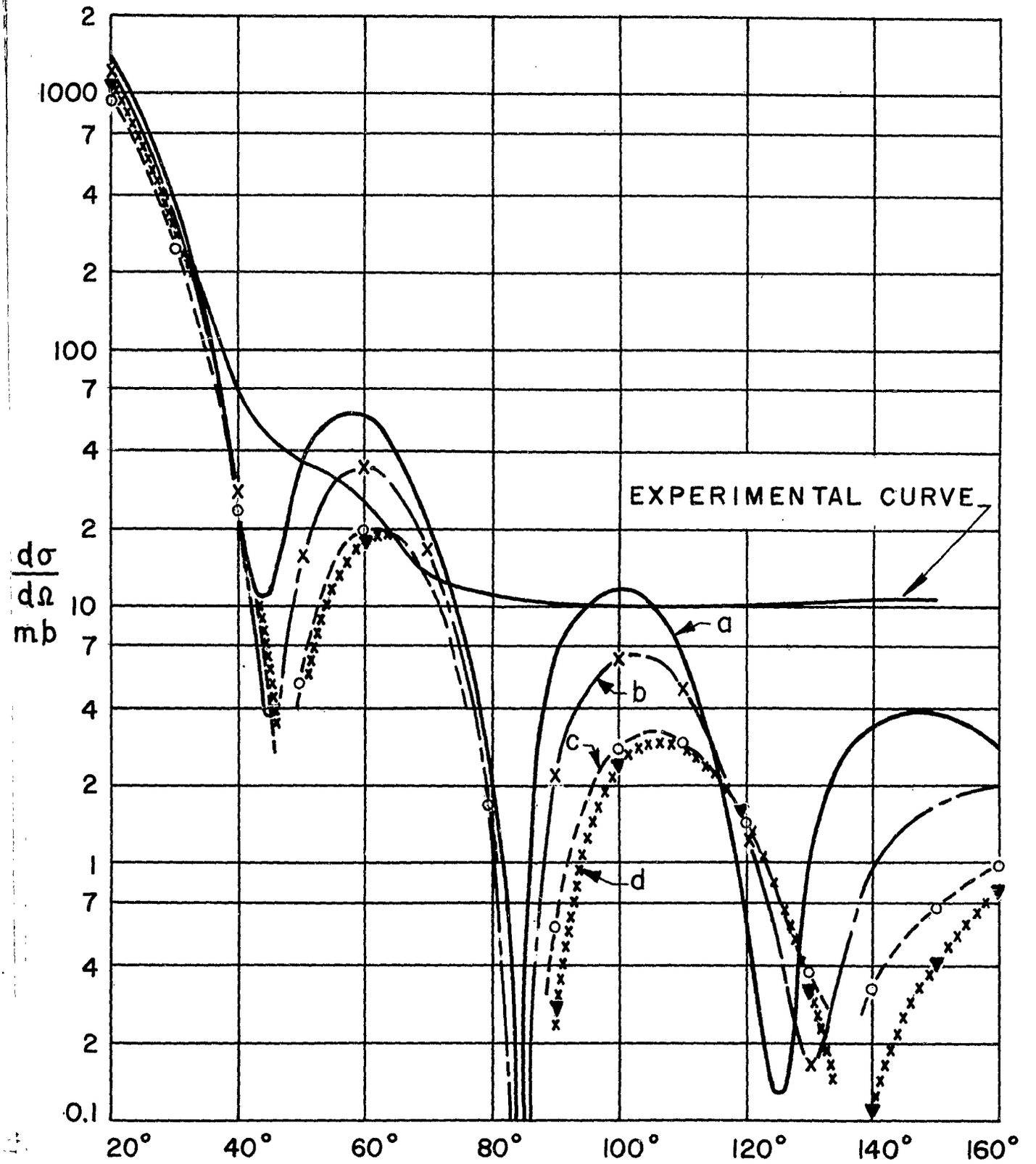
2
1000
7
4
2
100
7
4
2
10
7
4
2
1
7
4
2
0.1
dσ/dΩ mb
EXPERIMENTAL CURVE
a
b
c
d
20°
40°
60°
80°
100°
120°
140°
160°

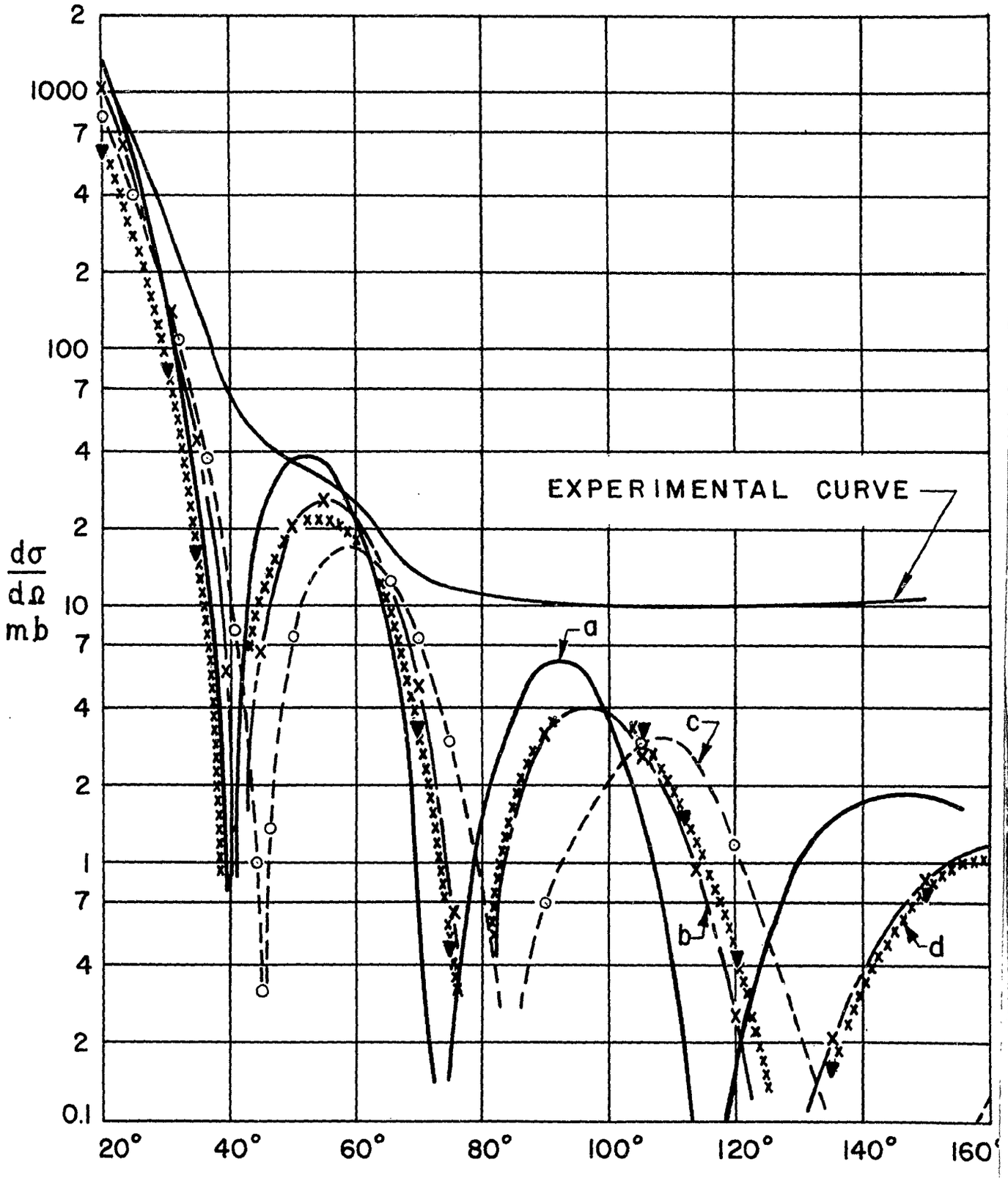
2
1000
7
4
2
100
7
4
2
10
7
4
2
1
7
4
2
0.1
dσ/dΩ mb
EXPERIMENTAL CURVE
a
b
c
d
20°
40°
60°
80°
100°
120°
140°
160°